

# Simulative investigation of rubber damper elements for planetary touch-down bearings

Benedikt SCHÜSSLER<sup>\*</sup>, Timo HOPF, and Stephan RINDERKNECHT

Technical University of Darmstadt, Institute for Mechatronic Systems, Germany

**Abstract.** Designing touch-down bearings (TDB) for outer rotor flywheels operated under high vacuum conditions constitutes a challenging task. Due to their large diameters, conventional TDB cannot suited well, and a planetary design is applied, consisting of a number of small rolling elements distributed around the stator. Since the amplitude of the peak loads during a drop-down lies close to the static load rating of the bearings, it is expected that their service life can be increased by reducing the maximum forces. Therefore, this paper investigates the influence of elastomer rings around the outer rings in the TDB using simulations. For this purpose, the structure and the models used for contact force calculation in the ANEAS simulation software are presented, especially the modelling of the elastomers. Based on the requirements for a TDB in a flywheel application, three different elastomers (FKM, VMQ, EPDM) are selected for the investigation. The results of the simulations show that stiffness and the type of material strongly influence the maximum force. The best results are obtained using FKM, leading to a reduction of the force amplitude in a wide stiffness range.

**Key words:** touch-down bearing; flywheel; drop-down simulation; rubber.

## 1. INTRODUCTION

Magnetic bearings gain more and more relevance in industrial applications. With the advantages of low losses and low maintenance as compared to rolling element bearings, high possible rotational speeds and functionality in a vacuum, magnetic bearings are perfectly suited for the implementation in flywheels. However, they also have some drawbacks, like the higher complexity and the need for a TDB in case of a malfunction or an overload, which has to be considered in the design of the flywheel. If the flywheel is built as an outer rotor type to increase energy density, the design of the TDB becomes even more complex, as the diameter of the TDB becomes very large. Quorck proposed a planetary TDB to decouple the rotor size from the TDB size [1]. In addition, the planetary design prevents the rotor from backward whirling in the TDB, which is a common problem in conventional TDB, especially for vertical rotors. In the planetary TDB, multiple bearing units are equally distributed circumferentially around the stator. One unit consists of two angular contact bearings and a roller, which touches the rotor in case of a drop-down. In [2], the capabilities of the new TDB design have been shown in simulations as well as in high speed drop-downs with a TDB test. Figure 1 shows the rotor and the planetary TDB, which is mounted in the stator of the previously mentioned test rig. The bearings used in the TDB unit are hybrid spindle bearings of the 6001 type with a vacuum grease (Krytox AB240).

As long as the surface speeds of the rotor and the bearings during a drop-down are different, high tangential forces occur

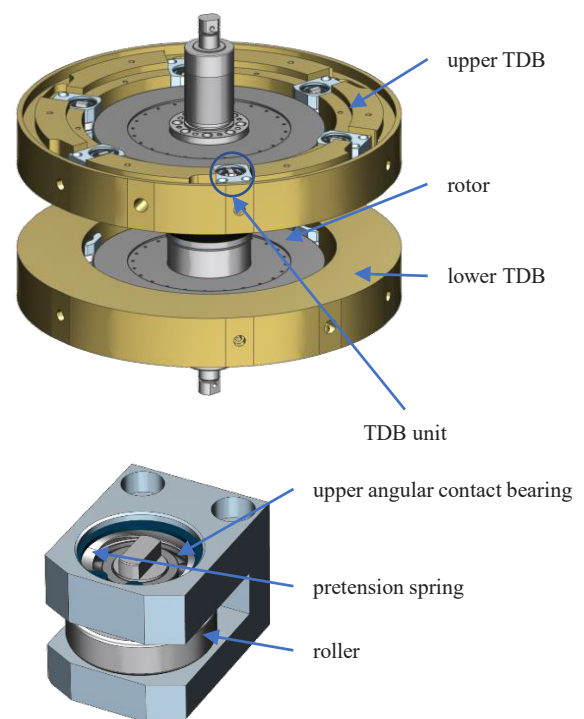


**Fig. 1.** Rotor of the TDB test rig with planetary TDB in the stator and a single TDB unit

due to the friction. These friction forces can lead to fast rotor movements, which result in high forces acting on the TDB. Therefore, one design criterion is small inertia for the bearings, so that they accelerate fast. Especially in the design of a planetary TDB with multiple small bearings, the tradeoff between bearing inertia and load capacity of the bearings has to be han-

<sup>\*</sup>e-mail: [schuessler@ims.tu-darmstadt.de](mailto:schuessler@ims.tu-darmstadt.de)

Manuscript submitted 2021-03-29, revised 2021-08-07, initially accepted for publication 2021-09-02, published in December 2021

dled carefully. If a bearing with a higher load rating is chosen, in general it becomes larger, too. This results in higher inertia. One possibility to mitigate the problem is by adding damping elements to reduce the forces. The positive effect for a conventional TDB has already been shown in [4] and [5]. Yili and Yongchun have shown that ideal stiffness and damping exist for which the forces in conventional TDB become minimal [6]. The authors are not aware of any literature addressing the effect of rubber dampers in planetary TDB as of today. Therefore, this paper analyses if the results for conventional TDB also apply to the planetary design. First, the requirements on the rubber damper in the flywheel application are analyzed. After that, the modelling of the material properties of the rubber dampers and the normal contact force calculation in the ANEAS simulation software (Analysis of Nonlinear Active Magnetic Bearing Systems) are described. Subsequently, simulation results for different material properties are shown before a short summary and conclusion are provided.

## 2. REQUIREMENTS RESULTING FROM FLYWHEEL APPLICATION

A common method for the integration of the rubber damper in the TDB is in the form of O-rings or rectangular rubber rings around the outer ring of the rolling element bearing. In the planetary design, it is also possible to mount the rubber ring between the rolling element and the inner ring of the bearing. However, the latter described integration has two disadvantages. First, the projected area is smaller and therefore the strain in the rubber would be higher and may destroy the rubber. The second reason are potentially high temperatures, which can also destroy the rubber. Experiments described in [3] show that the hottest temperature during drop-down tests occurs on the rolling element. Therefore, the favored position of integration is between the outer ring of the rolling element bearing and the housing.

There exists a variety of elastomers with very different characteristics and the possibility of different compounds applicable for one elastomer increases the variety further. However, there are also some very challenging demands for rubber dampers in TDB for flywheel applications. With the test rig described in [3] a temperature increase of 50 K to 100 K is measured at the outer races of the angular contact bearing during drop-down tests from full speed. With the requirements of a bearable temperature of 150°C and operation under high vacuum conditions, there are four elastomers especially suited for this purpose: EPDM (ethylene-propylene rubber), FKM (fluorocarbon rubber), FFKM (perfluorocarbon rubber) and VMQ (silicone rubber). Since the price for FFKM is much higher than for the other elastomers, the following investigation focuses on EPDM, FKM and VMQ.

## 3. MODELLING THE MATERIAL PROPERTIES OF ELASTOMERS

Due to their chemical structure divided by molecule chains, elastomers have a different material behavior than other materials conventionally used in mechanical engineering. The first

material characteristic is the hyperelasticity which leads to a nonlinear stress-strain relation for a quasi-static loading. There are different models, like the Neo-Hookean and the Mooney-Rivlin model. Because of the small airgap, maximum deformation is limited, so that the maximum deformation of the elastomer is distinctly lower than the thickness of the elastomer. As a result, a linearized model formed around the operating point can be used. Therefore, the relation between the stress  $\sigma$  and strain  $\varepsilon$  shown in (1) is used. In this relation, the elastic modulus  $E$  is independent of the strain. However, due to the second material characteristic, it depends on frequency  $\omega$ .

$$\sigma = E(\omega)\varepsilon. \quad (1)$$

This viscoelastic material behavior influences the dynamic behavior of the material and is of high relevance for this paper. Viscoelastic behavior means that, if the elastomer is set to a constant strain, stress decreases over time. If the elastomer is loaded with a harmonic stress, the response is harmonic, too. However, it has the phase delay  $\delta$  due to its viscoelasticity. This is shown in (2) and (3), where  $\hat{\sigma}$  and  $\hat{\varepsilon}$  are the amplitudes of stress and strain. The time is expressed by  $t$ .

$$\sigma = \hat{\sigma} e^{j(\omega t + \delta)}, \quad (2)$$

$$\varepsilon = \hat{\varepsilon} e^{j\omega t}. \quad (3)$$

With this formulation, the relation from (1) can be rewritten, as shown in (4). The complex elastic modulus  $|E(\omega)| e^{j\delta}$  is expressed by the sum of a real part, the storage modulus  $E'$ , representing the elastic stiffness, and an imaginary part, the loss modulus  $E''$ , representing the damping.

$$E(\omega) = \frac{\sigma}{\varepsilon} = |E(\omega)| e^{j\delta} = E'(\omega) + jE''(\omega). \quad (4)$$

These viscoelastic material properties are represented by the so-called master curves, which are determined in dynamic mechanical analyses. In Fig. 2 and Fig. 3, the master curves for the three materials investigated in this paper (EPDM E540-80; FKM V747-75; VMQ S604-70) are shown, based on the data given in [7]. In Fig. 2, the storage modulus is shown. It can be seen that for low excitation frequencies the storage modulus is very similar and varies by less than 100% between the materials. However, at high frequencies, the materials behave differently. For VMQ, the storage modulus increases by less than a decade, but for FKM, it increases by more than two decades. The loss factor for these materials, which is the loss modulus divided by the storage modulus, is shown in Fig. 3. This is a common way for representing dissipative material properties and it is especially suited for this paper, since stiffness can be varied by the geometry. Only the damping compared to the stiffness, which is expressed by the loss factor, is independent of the geometry. Like for the storage modulus, the material behavior for low frequency excitations of the three materials are similar, but for high frequency excitations, the material behavior varies a lot. VMQ has nearly no change in the loss factor while both FKM and EPDM have a peak. For FKM, this peak lies at lower frequencies and has a higher amplitude.

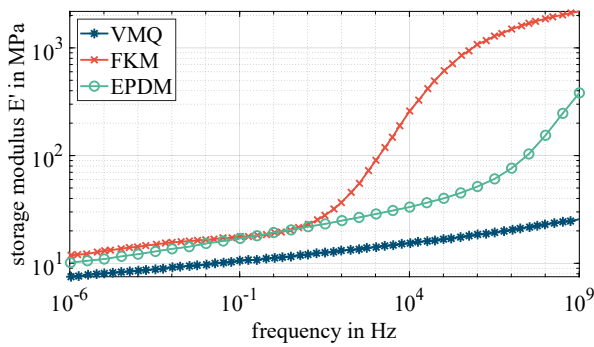


Fig. 2. Storage modulus of investigated materials [7]

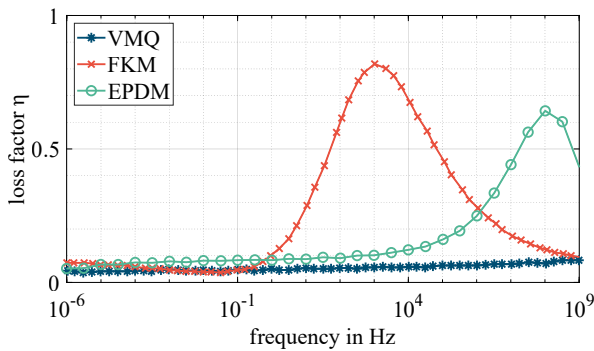


Fig. 3. Loss factor of investigated materials [7]

A suitable model to represent the viscoelastic characteristics of elastomers is a spring that is in parallel to a series of Maxwell elements, as shown in Fig. 4. Parameters  $E_k$  and  $\tau_k$  are called Prony parameters and can be fitted on the master curves. In order to do that, the Matlab based DMA2PRONY program is used. For determining the Prony parameters, only the frequency range between 1 Hz and 10 kHz is used for fitting the model, since it has the highest relevance for the dynamic simulation of drop-downs. Lower frequencies are only relevant for nearly static investigations and much higher frequencies are neglected due to the discretization of the solver in the simulations in the next step.

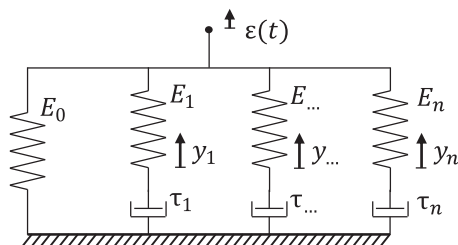


Fig. 4. Model for the dynamic stiffness of elastomers

With the Prony parameters, the non-constant elastic modulus can be calculated. For a uniaxial stress state, the time-dependent elastic modulus is given according to (5).

$$E(t) = E_0 + \sum_{k=1}^n E_k e^{-\frac{t}{\tau_k}}. \quad (5)$$

#### 4. MODELLING IN THE ANEAS SIMULATION ENVIRONMENT

ANEAS is a simulation tool to investigate the behavior in radial direction of magnetic bearing systems. It was developed by Orth [8] at the Technical University of Darmstadt. With ANEAS, it becomes possible to simulate both the rotor movement while it is levitated magnetically and the case of a drop-down in conventional TDB. However, only the radial movement can be investigated in the simulations. Later it was enhanced, as described in [2], to also support planetary TDB.

The first step in the modelling process is to find a model for the rotor and stator. The maximum rotational speed of the system is 333 Hz while the first bending frequency of the rotor stands at around 1700 Hz. Under normal operation, when the system is levitated by the active magnetic bearings, a rigid rotor and stator would therefore be sufficient. However, for the drop-down conditions investigated in this paper, flexible rotor and stator models are more appropriate. An impact which is exerted during the drop-down excites all eigenmodes and not only the ones close to the operating frequency. Even the static deformation of the stator fixed in the bottom and a force input at the upper TDB results in stiffness of  $10^9$  N/m, which is in the range of the contact stiffness described later. Due to these reasons, flexible rotor and stator models are used. The models are based on Timoshenko beam elements which are able to describe thick beams due to the considered shear deformation. To reduce the numerical effort during the simulation, these models are reduced based on the Hankel singular values. Therefore, only controllable and observable eigenmodes are kept for the simulation. The inputs are the forces in the TDB plane and the outputs are the positions in the TDB plane. Discretization of the model is performed as described in [2], since this model was already validated with experimental results. Because only the radial movement is considered, there is – if no TDB contact exists – only weak interaction between rotor and stator, resulting from negative stiffnesses of components such as the motor generator unit or the axial permanent magnetic bearing. In the case of coming into contact, these two systems are coupled by the contact forces, which are highly nonlinear. This contact force is calculated in every time step in the time domain simulation in ANEAS. It results from the contact stiffness in which the stiffness of the elastomer is only one stiffness in the force flow. Therefore, the following section describes the stiffnesses in the force flow and their calculation. The upper half of Fig. 5 shows the section view of a TDB unit with the force flow in blue and an orange dot at every point where stiffness is considered in the model. In the lower half, a schematic diagram of the stiffnesses is shown. Based on the deflection of the stator in the TDB plane,  $x_{\text{stator}}$  and the deflection of the rotor  $x_{\text{rotor}}$ , it is calculated if contact occurs. Relevant stiffnesses that are considered are in the elastomer, the bearing and the rotor-roller-contact. The stiffness of the roller bending and the deformation of the housing of the TDB unit are neglected, since they are considered large as compared to the other stiffnesses and therefore have only a small influence on overall stiffness. The bearing stiffness is mainly determined by the contacts between the inner race and the balls since they are contacts of convex bodies while the con-

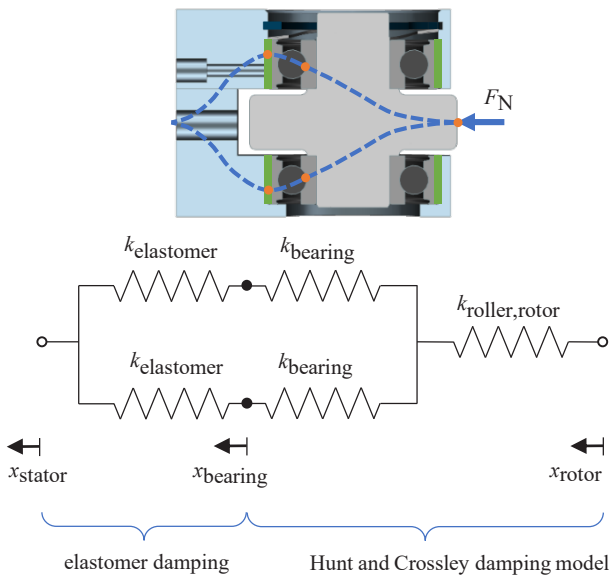


**Fig. 5.** Section view of a TDB and stiffness model of a single TDB unit

tacts between the outer race and the balls are contacts between concave bodies. The contact force  $F_N$  cannot only be calculated by the stiffnesses, but also has to be based on the damping of the system. In the material model of the elastomer, damping is already included while it has to be modelled for the contacts between the rotor and the roller as well as in the bearing separately with a more general approach according to Hunt and Crossley explained later.

If the rotor penetrates the stator, the contact between the rotor and the roller is considered to be a contact of two cylinders with parallel axes. Therefore, the simplification is made that it is a line contact and for the stiffness calculation, no tilting between the rotor and the roller occurs, which is a valid assumption due to the much higher length of the rotor as compared to the air gap between the rotor and the bearing. Based on the Hertzian theory, the stiffness of the rotor-roller contact is slightly nonlinear. However, due to the minor influence of this nonlinearity, the stiffness of the rotor-roller contact  $k_{\text{roller, rotor}}$  is calculated according to (6) as linear stiffness [9]. The contact length between the two cylinders given by  $l$  and  $\nu$  is the Poisson ratio while  $E$  is the elastic modulus of the rotor respectively to the roller.

$$k_{\text{roller, rotor}} = \frac{\frac{\pi l}{4}}{\frac{1 - \nu_{\text{rotor}}^2}{E_{\text{rotor}}} + \frac{1 - \nu_{\text{roller}}^2}{E_{\text{roller}}}}. \quad (6)$$

The stiffness of the bearing, which is an angular contact bearing, is based on the equation developed by Gargiulo [10] and is shown in (7). The stiffness depends on the number of balls  $Z$ , the mean diameter of the bearing  $D_m$  and the contact angle  $\alpha_b$  of the angular contact bearing. Since it is a nonlinear stiffness, it depends also on the compression of bearing  $\bar{x}_b$ .

$$k_{\text{bearing}} = 3.312 \cdot 10^{10} Z \sqrt{D_m (\cos(\alpha_b))^5 \bar{x}_b}. \quad (7)$$

The damping of the rotor-roller-contact and the contact in the bearings is complex and not exactly known. Therefore, a more general approach based on the model by Hunt and Crossley (HC) [11] is used. Compared to other dissipative contact force models, such as the Kelvin–Voigt model, the HC model has the advantage of continuity and positive contact forces during the whole contact, which is more realistic. According to this model, the dynamic contact force  $F_N$  is based on the static force  $F_{N,\text{static}}$  to which a portion proportional to the deformation velocity  $\dot{\delta}$  is added as shown in (8). The damping coefficient  $\alpha$  is calculated based on (9). It depends on the velocity at the beginning of the contact  $\dot{\delta}^-$  and the coefficient of restitution  $COR$ , which is considered for a steel-steel-contact to be 0.75. This value is in the range shown in [12].

$$F_N = F_{N,\text{static}} \left( \frac{3}{2} \alpha \dot{\delta} + 1 \right), \quad (8)$$

$$\alpha = \frac{1 - COR}{\dot{\delta}^-}. \quad (9)$$

The stiffness of the rectangular elastomer rings depends on the elastic modulus and on the geometry of the rings. Bormann [7] gives the stiffness for a rectangular ring  $k_{\text{elastomer}}$  with no contraction at the inner and outer contacting surfaces and a plane stress state according to (10). The condition of no contacting surfaces can be fulfilled by vulcanization of the rings to the surfaces. The geometry of the ring is defined by the mean diameter  $D_{E,m}$ , the width  $w$  and the height  $h$  of the ring.

$$k_{\text{elastomer}} = \pi D_{E,m} E(t) \frac{w}{6h} \left( 5 + \left( \frac{w}{h} \right)^2 \right). \quad (10)$$

From the different stiffnesses of the TDB, the contact stiffness and the bearing stiffness can hardly be changed because it would affect overall geometry. In contrast to that, geometry of the rectangular elastomer ring can be changed to a large extent. Either the width of the ring or the height can be changed. In addition to that, dynamic stiffness is also influenced by the material properties. Therefore, a simulation study is conducted to find an optimum geometry and material for the TDB of the TDB test rig.

## 5. SIMULATION STUDY DESIGN

The goal of the simulation study is to find the best suited material along with optimum stiffness of the elastomer to reduce the loads on the TDB. For this reason, simulations are conducted without and with elastomer rings in the TDB and subsequently compared to each other.

### 5.1. Simulation study design

A reference set is used as reference for the comparison and in order to quantify the improvement. In the set with the elastomers, the three previously described elastomers are used. Since a drop-down in planetary TDB is close to showing chaotic behavior, multiple simulations are conducted with only a slight change in the initial conditions. Table 1 shows the values for

the varied initial conditions. For both sets, two main rotational speeds were investigated, i.e. 13 000 rpm and 20 000 rpm. For all sets of simulations, the initial translational speed also varied slightly. Since the reference set is used as the basis for the comparison, a scatter in these simulations can introduce a major error. To cope with this scatter in the reference set, the initial rotational speed is changed slightly, too. Simulations are conducted for all combinations of these two parameters.

**Table 1**

Varied initial conditions for the reference set and the elastomer test

simulation	initial rotational speed in rpm	initial translational speed in m/s
reference	13 000, 13 001, 13 002, 20 000, 20 001, 20 002	0.05, 0.049
with elastomer	13 000, 20 000	0.05, 0.049

The highest loads occur in the phase where the rotor moves fast in the TDB and synchronizes the surface speed of the TDB units with the rotor surface speed. To analyze the drop-downs and compare them to each other, it must be ensured that the synchronization phase is passed during the simulation. For most simulations, this happens in the first five seconds. However, from previously conducted simulations an integration time of 15 s has shown to be a reasonable choice. The drop-down speed of 20 000 rpm is the highest possible speed of the TDB test rig, which results in a surface speed of 230 m/s in the TDB plane. The loads on the TDB generally increase with the drop-down speed. The speed of 13 000 rpm is only investigated to rule out more fatal drop-downs due to unexpected behavior at lower drop-down speeds. However, the simulation results show the expected behavior, as for most simulations the loads at 13 000 rpm were lower than at 20 000 rpm, and only for a few simulations the parameter showed slightly more severe results for the lower speed. This can be explained with the chaotic behavior of the system. Therefore, the following evaluations focus on the drop-down simulations with an initial speed of 20 000 rpm.

For the simulation study, a reasonable range for the stiffness variation of the elastomer had to be found. The upper limit of the stiffness is defined by geometric constraints. The highest stiffness is reached when the complete outer ring is surrounded by the elastomer ring, which means that the width of the elastomer ring is equal to the bearing width and in addition, the height has to be the lowest available height of 0.5 mm. According to (10), this results in a static stiffness value of  $10^9$  N/m. The lower limit is chosen more freely, but if the height of the ring becomes much higher than the width, it is not applicable very effectively, which defines a lower static stiffness limit of around  $0.5 \cdot 10^6$  N/m.

In order to keep the simulation effort low, eight stiffnesses in the above-mentioned range are simulated in a first run with the initial conditions presented in Table 1. Based on the results, the stiffness range is adjusted, and a finer stiffness discretization is used for a second run. The relevant stiffness range is

determined by the maximum penetration depth. In general, the maximum penetration of the rotor in the stator increases with a decrease in the stiffness. A more detailed analysis of the penetration is shown in Section 5.3. If the penetration becomes too high, there is the risk of unwanted rotor-stator-contact in a real system. This cannot happen in the simulation, because only the coupling of the rotor and stator at the TDB is modelled. Therefore, only the stiffness range with a penetration depth below 150  $\mu\text{m}$  resulting in a total displacement of 430  $\mu\text{m}$  is used for the second simulation run. As a result, the stiffness range investigated in the second simulation run is different for each material. The investigated stiffnesses are shown in Table 2.

**Table 2**

Stiffnesses investigated in the two simulations sets

material	stiffnesses first simulation run in $10^6$ N/m	stiffnesses second simulation run in $10^6$ N/m
FKM	0.5, 1, 5, 10, 50, 100, 500, 1000	6, 7, 8, 9, 20, 30, 40, 60, 70, 80, 90, 200, 300, 400, 600, 700, 800, 900
VMQ	0.5, 1, 5, 10, 50, 100, 500, 1000	200, 300, 400, 600, 700, 800, 900
EPDM	0.5, 1, 5, 10, 50, 100, 500, 1000	60, 70, 80, 90, 200, 300, 400, 600, 700, 800, 900

## 5.2. Analysis of exemplary simulation results

First, the simulation results from an exemplary drop-down simulation are shown and analyzed. The chosen simulation uses an FKM elastomer ring with the smallest investigated stiffness, a drop-down speed of 20 000 rpm and an initial velocity of 0.049 m/s. Fig. 6 shows the rotational speed of the rotor and the bearings (B) in the lower TDB. The rotational speed of the bearings is multiplied by the ratio of the roller diameter and the rotor diameter. The drop-down can be divided into three phases due to the different behavior of the rotor. In the first phase, from 0 s to around 2 s, the acceleration of the bearings in the TDB is low. In this phase, the rotor jumps in the TDB, so that there is only an acceleration while the rotor hits the TDB units. Until the next hit the TDB units decelerate almost to a standstill. In the second phase, i.e. the synchronization phase, the rotor accelerates the bearings until the contacting surfaces have the same surface speed. It can be seen that the bearings accelerate rapidly while the rotor decelerates rapidly, which is due to the energy transfer from the rotor to the bearings. In this phase, the translational velocity of the rotor is higher than in the other phases, which is shown in Fig. 7. The increase in the translational velocity is due to the friction force which leads to a whirling motion. The duration of this phase in this simulation is approximately 1 s. After all bearings have been accelerated, the synchronization is finished and the final phase starts. In this phase, the rotor moves slowly in the TDB. Therefore, the bearings decelerate a bit before they are again accelerated to the synchronous rotor speed. However, the tangential force during these contacts is too small to create a whirling motion.

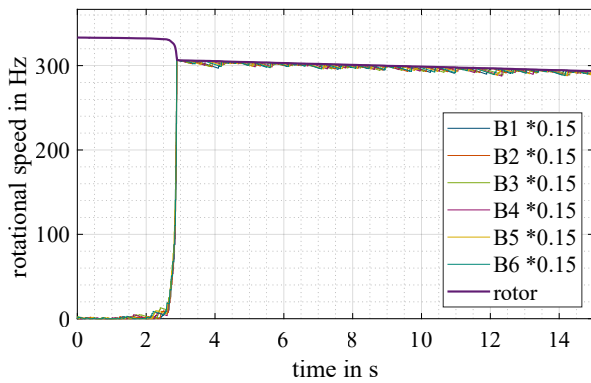


**Fig. 6.** Rotational speed of the rotor and the bearings in the lower TDB for simulation with FKM for the lowest investigated stiffness, 20 000 rpm and initial velocity of 0.049 m/s

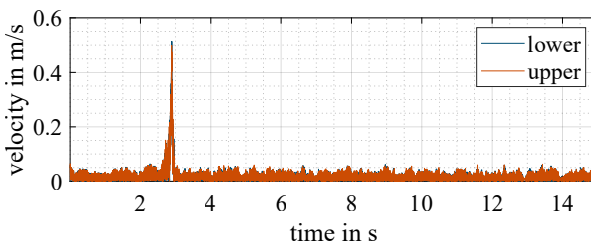


**Fig. 7.** Translational velocity of the rotor for simulation with FKM for the lowest investigated stiffness, 20 000 rpm and initial velocity of 0.049 m/s

The whirling motion is also clearly visible in the orbit plot in Fig. 8, which shows the rotor movement relative to the stator movement in the TDB planes. However, it is not a whirling motion known from conventional TDB. The rotor does only about ten revolutions in the TDB before the second phase ends and the rotor slows down. The frequency at which the rotor whirls is around 90 Hz and therefore lower than the first eigenfrequency of the coupled rotor-stator-system. In Fig. 7 it can be seen that the rotor is still accelerating at the end of the synchronization phase, but this is no steady whirling motion.

This previously described rotor behavior with the three phases can be seen in all simulations regardless whether elastomer rings are used or not. The difference is that in some simulations, the peak in the velocity is not as dominant as in Fig. 7 and the synchronization phase has a longer duration. In these simulations, the whirl is also not as distinct as in Fig. 8. In Fig. 9, the orbit of the system with FKM rings with the highest investigated stiffness is shown. Even in this stiff TDB, the rotor does one revolution in the TDB with higher penetrations. The penetration is higher at one side of the clearance boundaries, which can be explained by the backward whirling character. The rotation of the rotor is counterclockwise, resulting in a clockwise movement of the rotor in the TDB due to the friction force. Therefore, if the rotor moves along the clearance boundaries, the penetration of the first contact to the next TDB unit is higher. During the whirling motion, the whirling frequency is below the first eigenfrequency of the coupled rotor-stator-system, like in all other simulations.

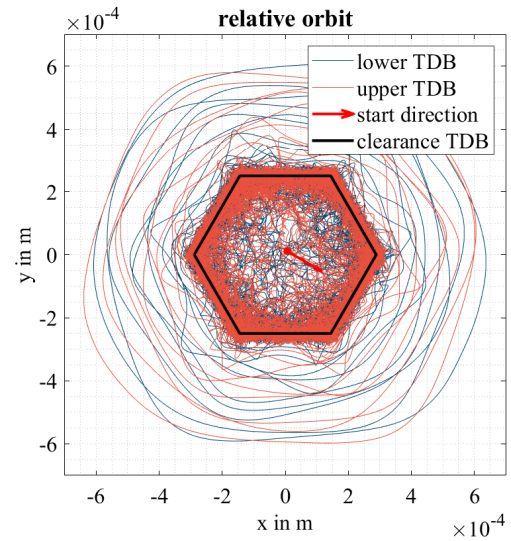


**Fig. 8.** Orbit plot for simulation with FKM for the lowest investigated stiffness, 20 000 rpm and initial velocity of 0.049 m/s

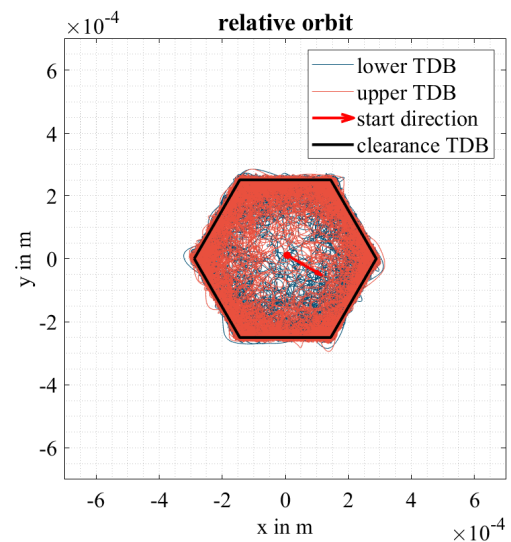


**Fig. 9.** Orbit plot for simulation with FKM for the highest investigated stiffness, 20 000 rpm and initial velocity of 0.049 m/s

### 5.3. Displacement analysis

As described at the beginning, the task of the TDB is to prevent rotor-stator-contact elsewhere than at the TDB. Therefore, the total displacement resulting from the air gap and the deformation due to the contact forces must be the smallest air gap of the system. Usually, TDB clearance is half of the clearance of other components. In the case of the TDB test rig, the nominal air gap is 280  $\mu\text{m}$  with a 6-element planetary TDB. To find an optimum design, the simulation results are analyzed in a first step concerning the maximum displacement of the rotor. In Fig. 10, the maximum displacements for the different simulations for the investigated elastomers and for simulation without elastomers are shown. For all elastomer materials, there is a stiffness at which the maximum displacement increases significantly. As previously explained, only stiffnesses higher than the point at

which the displacements exceed 430  $\mu\text{m}$  are selected for the second simulation run. The fact that there is a point where the displacement increases so rapidly can be explained by the unstable characteristics, with higher displacements leading to higher eccentricities and therefore to higher forces during a whirling motion. For low stiffnesses, the whirl suppressing character of the planetary TDB becomes weaker.

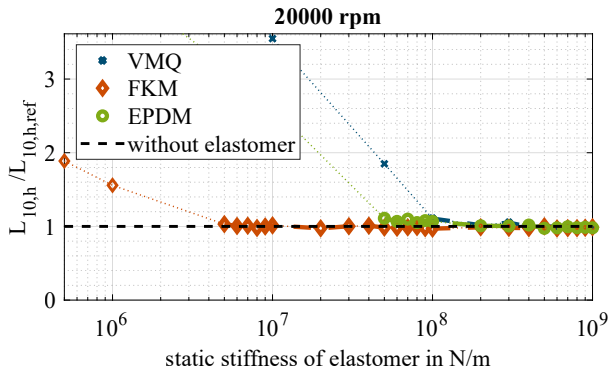


Fig. 10. Maximum displacement of the rotor relative to the stator

#### 5.4. Analysis of results with severity indicators

To analyze the simulation results further, different severity indicators can be used. One possibility is the maximum force. If the maximum force is much higher than the static load rating of the bearing, immediate bearing failure can be expected. Experiments with the TDB test rig described in [3] showed that the bearing withstands multiple contacts with nearly double the static load rating of the bearing without immediate failure. A load above the static load rating leads under static conditions to plastic deformation of the bearing races. However, even if the occurring deformation due to the exceedance of the static load rating does not lead to immediate failure, it is not favorable for the bearing service life. Under dynamic load, the bearable force before plastic deformation occurs is higher. For contact durations of around 0.002 s, which is typical for the investigated drop-downs, the bearable force under dynamic loads is 1.1 to 1.6 times higher as compared to a static load [13]. Since the exact value is not precisely known, the goal is to keep peak loads below the static load rating. Figure 11 shows the maximum normal force on the TDB unit. It can be seen that even for the sim-

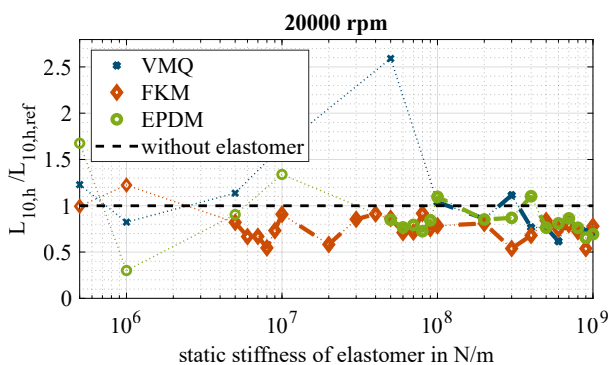


Fig. 11. Maximum normal force on the TDB unit

ulations where the displacements became high, there is not necessarily an increase in the normal forces. The simulation with the lowest normal force is the simulation with FKM elastomers with stiffness of  $8 \cdot 10^6$  N/m. Except for four simulations, the maximum forces in the acceptable displacement range were below the forces in the reference simulations. For FKM, all simulation results in the stiffness range higher than  $5 \cdot 10^6$  N/m show a lower maximum force than the reference simulations.

Another severity indicator which can be used to analyze the drop-down simulations and compare them to each other is the bearing service life. Compared to the severity indicator of the maximum force shown before, it does not use single values but takes the whole drop-down into account. Therefore, this value considers the wear-out instead of immediate failure. The classical bearing service life for angular contact bearings  $L_{10,h}$  is calculated with (11). In this equation,  $n_m$  expresses the mean rotational speed in rpm,  $C$  is the dynamic load rating, i.e. a parameter given in the datasheet of the bearings, and  $P_m$  stands for the mean equivalent bearing load.

$$L_{10,h} = \frac{10^6}{60n_m} \left( \frac{C}{P_m} \right)^3. \quad (11)$$

Calculation of the mean equivalent load  $P_m$  for dynamic transient loads such as during drop-downs is done according to (12) [14]. Index  $i$  denotes the current time step of the simulation up to the last time step  $ts$ . The length of the time step related to the overall evaluation time is given by  $q_i$ . The bearing speed in rpm of the current time step is expressed by  $n_i$ . In this equation, the normal force is divided by two because the force flow is expected to be split equally on both bearings, as described before.

$$P_m = \sqrt[3]{\frac{\sum_{i=1}^{ts} q_i n_i \left( \frac{F_{N,i}}{2} \right)^2}{n_m}}. \quad (12)$$

In the literature it is mentioned that the classical bearing service life calculation is unable to predict the service life of the bearings correctly [15]. In [16], the classical bearing service life calculation is adapted to be used for TDB drop-downs. However, this adapted bearing service life prediction has not been validated in experiments. For this reason, this paper uses the classical bearing service life calculation shown in (11) for the comparison of different drop-downs. Since the absolute value is not representative, the severity indicator used in this paper consists of the bearing service life of the investigated simulation divided by the bearing service life of the reference simulation  $L_{10,h,ref}$ . The bearing with the smallest value in the TDB was always taken as value for the bearing service life. A value greater than one means that the service life of the TDB is higher than that of the reference simulation, and, respectively, a value smaller than one means reduced service life as compared to the reference simulation. In Fig. 12, the bearing service life of the different simulations related to the reference simulation are shown. For high stiffnesses, the calculated related bearing service life is for all simulations greater than one, which means

service life improvement as compared to the reference simulation. For VMQ and EPDM, there is the tendency for the bearing service life to increase with the stiffness. For FKM, there is no tendency in the stiffness range higher than  $5 \cdot 10^6$  N/m where also the displacements are acceptable. However, all stiffnesses in the applicable range besides two stiffness values for FKM show the highest related bearing service life, and for VMQ for all besides two the lowest related bearing service life is noted. With FKM elastomer dampers, the bearing service life can be increased by 50% on average.

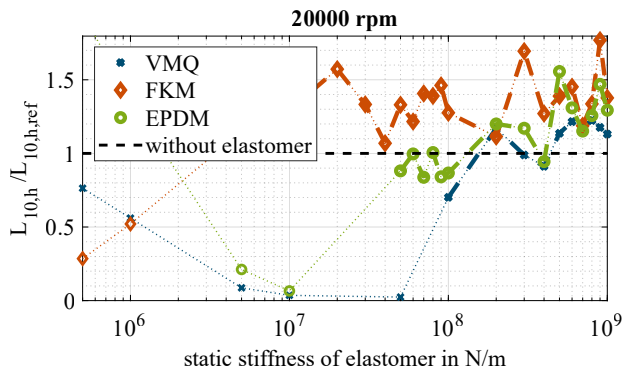


Fig. 12. Related bearing service life for different simulations

## 6. CONCLUSIONS

The paper investigates if elastomers are suited as damping elements for flywheel applications. Based on the three materials, i.e. VMQ, FKM and EPDM, a modelling approach for dynamic stiffness of elastomers is shown. The Prony parameters, which are the model parameters, are obtained from the master curves of the materials. Based on this model, the elastomer rings are implemented in the overall stiffness model in the ANEAS simulation environment. In addition to this elastomer stiffness, also the modelling of other stiffnesses affecting the contact stiffness is shown. Simulations with different materials are conducted for different static stiffnesses of the elastomers and different initial conditions. For the evaluation, maximum displacement as well as maximum force and the bearing service life are all considered.

The simulation results indicate that FKM is best suited as a damping element in TDB application. The preferable stiffness ranges from  $5 \cdot 10^6$  N/m to the maximum possible stiffness of  $10^9$  N/m. In the real system, this could be an elastomer ring surrounding the complete outer ring of the bearing with a height between 0.5 mm and 3 mm. The maximum forces, acting as peak load indicators, can be lowered by 43% and the bearing service life, as a wear-out indicator, can be increased by up to 77%. The fact that FKM is the best-suited elastomer while VMQ is less suited than EPDM and FKM can be explained by the loss factor. FKM has the highest loss factor, and the peak of the loss factor is in the most relevant frequency range while EPDM has the peak at higher frequencies and VMQ has no peak in the loss factor. This indicates that high damping as compared to the stiffness is preferable. In [17], a theoretical analysis was performed, showing for conventional TDB that if the damping

gets too high, the backward whirl is enabled again, which leads to high loads, too. However, in this paper, which investigated materials in planetary TDB, no such effect has been seen.

The application of elastomer dampers has additional advantages. Additional stiffness leads to lower force peaks if there are imperfections on the raceways. These imperfections can result, for example, from damage occurring during assembly or adhesion on the rotor raceway from the roller. Since the simulation is based on idealized assumptions, these effects were not modeled in the simulation.

However, before the elastomer rings are applied to the test rig, additional studies concerning the thermal effects have to be conducted. Since the test rig is operated under high vacuum conditions, heat transmission is only possible by heat conduction and radiation. The heat generated in the TDB unit is mainly transmitted to the main stator parts by conduction which will flow through the elastomer, since the effect of radiation is low. With the elastomer rings in the TDB unit, thermal resistance increases and temperature in the TDB unit will increase, too. Even if this temperature increase is bearable for the elastomer, it has to be investigated in further studies.

## ACKNOWLEDGEMENTS

This research work was supported by the Federal Ministry for Economic Affairs and Energy on the basis of a decision by the German Bundestag.

## REFERENCES

- [1] L. Quurck, H. Schaede, M. Richter, and S. Rinderknecht, "High Speed Backup Bearings for Outer-Rotor-Type Flywheels – Proposed Test Rig Design," in *Proceedings of ISMB 14*, Linz, Austria, 2014, pp. 109–114.
- [2] L. Quurck, D. Franz, B. Schübler, and S. Rinderknecht, "Planetary backup bearings for high speed applications and service life estimation methodology," *Mech. Eng. J.*, vol. 4, no. 5, 2017, doi: [10.1299/mej.17-00010](https://doi.org/10.1299/mej.17-00010).
- [3] L. Quurck, R. Viitala, D. Franz, and S. Rinderknecht, "Planetary Backup Bearings for Flywheel Applications," in *Proceedings of ISMB 16*, Beijing, China, 2018.
- [4] J. Cao, P. Paul Allaire, T. Dimond, C. Klatt, and J.J.J. van Rensburg, "Rotor Drop Analyses and Auxiliary Bearing System Optimization for AMB Supported Rotor/Experimental Validation – Part II: Experiment and Optimization," in *Proceedings of ISMB 15*, Kitakyushu, Japan, 2016, 819–825.
- [5] J. Schmied and J.C. Pradetto, "Behaviour of a One Ton Rotor being Dropped into Auxiliary Bearings," in *Proceedings of ISMB 3*, Zürich, Schweiz, 1992, pp. 145–156.
- [6] Z. Yili and Z. Yongchun, "Dynamic Responses of Rotor Drops onto Auxiliary Bearing with the Support of Metal Rubber Ring," *Open Mech. Eng. J.*, vol. 9, no. 1, pp. 1057–1061, 2015, doi: [10.2174/1874155X01509011057](https://doi.org/10.2174/1874155X01509011057).
- [7] A. Bormann, *Elastomerringe zur Schwingungsberuhigung in der Rotordynamik: Theorie, Messungen und optimierte Auslegung*. Dissertation. Düsseldorf: VDI-Verl., 2005.
- [8] M. Orth and R. Nordmann, "ANEAS: A Modeling Tool for Nonlinear Analysis of Active Magnetic Bearing Systems," *IFAC Proceedings Volumes*, vol. 35, no. 2, pp. 811–816, 2002, doi: [10.1016/S1474-6670\(17\)34039-9](https://doi.org/10.1016/S1474-6670(17)34039-9).

## Simulative investigation of rubber damper elements for planetary touch-down bearings

- [9] V.L. Popov, *Contact Mechanics and Friction: Physical Principles and Applications*. Berlin, Heidelberg: Springer, 2017.
- [10] E.P. Gargiulo Jr., "A simple way to estimate bearing stiffness," *Machine Design*, vol. 52, no. 17, pp. 107–110, 1980.
- [11] K.H. Hunt and F.R.E. Crossley, "Coefficient of Restitution Interpreted as Damping in Vibroimpact," *J. Appl. Mech.*, vol. 42, no. 2, p. 440, 1975, doi: [10.1115/1.3423596](https://doi.org/10.1115/1.3423596).
- [12] M.C. Marinack, R.E. Musgrave, and C.F. Higgs, "Experimental Investigations on the Coefficient of Restitution of Single Particles," *Tribol. Trans.*, vol. 56, no. 4, pp. 572–580, 2013, doi: [10.1080/10402004.2012.748233](https://doi.org/10.1080/10402004.2012.748233).
- [13] R.J. Mainstone, "Properties of materials at high rates of straining or loading," *Mat. Constr.*, vol. 8, no. 2, pp. 102–116, 1975, doi: [10.1007/BF02476328](https://doi.org/10.1007/BF02476328).
- [14] H. Wittel, D. Muhs, D. Jannasch, and J. Voßiek, "Wälzlager und Wälzlagerungen," in *Roloff/Matek Maschinenelemente*, H. Wittel, D. Muhs, D. Jannasch, and J. Voßiek, Eds., Wiesbaden: Vieweg+Teubner Verlag, 2009, pp. 475–525.
- [15] J. M. Gouws, "Investigation into backup bearing life using delevitation severity indicators," North-West University, Potchefstroom, South Africa, 2016.
- [16] G. Sun, "Auxiliary Bearing Life Prediction Using Hertzian Contact Bearing Model," *J. Appl. Mech.*, vol. 128, no. 2, p. 203, 2006, doi: [10.1115/1.2159036](https://doi.org/10.1115/1.2159036).
- [17] T. Ishii and R. G. Kirk, "Transient Response Technique Applied to Active Magnetic Bearing Machinery During Rotor Drop," *J. Vib. Acoust.*, vol. 118, no. 2, pp. 154–163, 1996, doi: [10.1115/1.2889643](https://doi.org/10.1115/1.2889643).